JOURNAL OF GUIDANCE, CONTROL, AND DYNAMICS
Vol. 15, No. 5, September-October 1992

Dynamics and Control of Maneuverable Towed Flight Vehicles

J. E. Cochran Jr.,* M. Innocenti,† T. S. No,‡ and A. Thukral‡
Auburn University, Auburn, Alabama 36849

This paper considers the problems of dynamically modeling and automatically controlling the motion of a small maneuverable flight vehicle that is being towed by a much larger one. Mathematical models of the components of the system, including the towing aircraft, tow cable reel mechanism, tow cable, and vehicle aerodynamics, are described. The development of an autopilot for stability augmentation and maneuvering of the towed vehicle is discussed. An overview of the implementation of the models in a digital computer simulation program is provided, and some typical results obtained using the program are presented. A comparison of theoretical and experimental results is also made.

I. Introduction

FROM the early days of powered flight, there has been an interest in towing objects from aircraft. Objects that have been towed include antennas, banners, gliders, and targets. Because of the interesting, and sometimes troublesome, characteristics of the motions of some towed objects and the cables, or towlines, the dynamics of the cables and the towed objects have been studied by several investigators at various times during the last 60 years.[1-10]

The problem of describing the motion of a towed cable/object system is far from trivial. The equations of motion are, in general, coupled, ordinary, and partial differential equations (i.e., hybrid equations). Various approaches have been taken in studying such systems. Glauert[1] and Phillips[2] did some pioneering work on the stability of the motion of bodies towed from aircraft. Phillips[3] also analyzed the stability of the motion of a cable used to tow a nonlifting body. He used a continuum model for the cable and studied the effects of towing speed on the stability of lateral oscillations of the cable and concluded that the oscillations would be damped out if the speed of flight were less than the speed of propagation of vibrational waves along the cable.

During the late 1960s and early 1970s, interest in obtaining a more complete description of the dynamics of tow systems consisting of a towing aircraft, a cable, and a towed object, led to articles and reports (see Genin and Canon,[4] Norman et al.,[5] Huffman and Genin,[6] Huang,[7] DeLaurier[8] and Cannon and Genin[9]) that added a great deal to the general understanding of the problem. The analysis of DeLaurier[8] is perhaps the most comprehensive stability analysis to date. None of these efforts, however, produced a means for simulating, in an effective way, the motion of a towed vehicle system. A principal impediment to progress during this period was that the computers of that era were too slow to provide extensive numerical results with reasonable expenditures for computer time when continuous, or high-degree-of-freedom, lumped-mass models for the cable were used.

The availability of fast, economical computing hardware and more efficient numerical algorithms has spurred renewed interest in dynamics problems involving cables and tethers. Reference 10, for example, deals with the simulation of the nonlinear motion of a tethered, lighter-than-air vehicle. Related work in the area of tethered satellite dynamics[11-13] also forms a portion of the basis for further work in this area. Except for the tow system of Ref. 5, in which the towed vehicle is modeled as a point mass, the towed object has been considered as a passive body. Usually, the towed vehicle is also considered nonlifting. Moreover, most analysis and numerical results have been restricted to planar motion. Thus, although a good deal of work has been done, there is still a need for modeling, analysis, and simulation of tow systems in which the towed vehicle is maneuverable.

In this paper we consider the problems of dynamically modeling a tow system and designing a system for automatically controlling the towed vehicle. In the process of addressing this problem, we have developed a relatively general digital simulation of a system consisting of a towing aircraft, the tow cable reel, the cable, and a maneuverable towed vehicle.[14] Modeled dynamically as a rigid body, the towed vehicle is assumed to contain a stability and control augmentation system (SCAS) that allows the basic vehicle to be inherently less statically stable than conventional targets. Hence, not only can the target be maneuvered, but also its flight characteristics can be tailored to represent a variety of vehicles of interest. The simulation is both theoretically and practically useful and has been used in the development of the first maneuverable tow target to be flown *above* the towing aircraft and successfully recovered.[15]

In the following, we first describe the mathematical models for the towing aircraft, the cable, the towed vehicle, and the SCAS. Second, we explain the general structure of the simulation. Third, we present some results to illustrate the usefulness of the simulation. Fourth, we present a brief comparison of our theoretical results with the experimental results of Ref. 8.

II. Mathematical Models

General Description

In our development of the present models we have assumed that the towing vehicle is much larger than the towed vehicle so that the towing aircraft's motion is unaffected by the towed vehicle and may be specified a priori. The tow cable is modeled as a system of n point masses connected by massless, straight cable segments. Aerodynamic and gravitational forces that act on the masses are determined from physical and aerodynamic characteristics of cable segments. The number of masses used is arbitrary (but, of course, limited) to allow for variations in the length of the cable during deployment and retrieval. The segments between point masses on the cable are assumed to be inextensible. However, the length of the segment between the mass closest to the aircraft may vary in length. The center of mass towed vehicle is controlled using movable aerodynamic surfaces (e.g., elevators, rudder, and ailerons). It is modeled

Received July 5, 1990; presented as Paper 90-2841 at the AIAA Atmospheric Flight Mechanics Conference, Boston, MA, Aug. 14-16, 1990; revision received July 12, 1991; accepted for publication Oct. 17, 1991.

*Professor, Department of Aerospace Engineering. Associate Fellow AIAA.

†Associate Professor, Department of Aerospace Engineering. Senior Member AIAA.

‡Graduate Research Assistant, Department of Aerospace Engineering. Student Member AIAA.

dynamically as a single rigid body; i.e., movement of the control surfaces is assumed to affect the motion of the vehicle only indirectly through resulting changes in the aerodynamic reactions.

System Geometry

Four dextral orthogonal coordinate systems are used in defining the basic geometry of the system (see Figs. 1 and 2). The *EXYZ* system is fixed to the Earth's surface with its *Z* axis directed vertically down (a flat Earth is assumed) and its *X* axis directed along the horizontal projection of the initial velocity of the towing aircraft. The *EXYZ* system serves as our inertial reference. The $Ax_Ay_Az_A$ system is fixed in the towing aircraft with its origin at the aircraft's center of mass. The x_A axis is the longitudinal axis of the towing aircraft, and the y_A axis is directed out the right side of the aircraft. Point *P* shown in Fig. 1 is the point of attachment of the tow cable to the aircraft. The position vector $\boldsymbol{r}_P$ locates *P*, and its velocity and acceleration are $\boldsymbol{v}_P$ and $\boldsymbol{a}_P$, respectively. The vehicle's center of mass *C* is the origin of both the local vertical system $Cx_vy_vz_v$ and the target-fixed (body-fixed) system, *Cxyz* (see Fig. 2). Unit vectors, $\hat{i}, \hat{j}$, and $\hat{k}$ are associated with the *Cxyz* system.

A local coordinate system, $m_{j+1}x_jy_jz_j$, is defined for each point mass m_j (see Fig. 3). For the *n*th mass we have $px_ny_nz_n$. The towed vehicle is mass m_1. Unit vectors $\hat{\boldsymbol{e}}_{ij}$ $(i=1,2,3)$ are associated with the coordinate systems $m_{j+1}x_jy_jz_j$ and $Px_ny_nz_n$. The attitude of the *j*th segment of cable, with respect to *EXYZ*, is defined by the angles θ_{1j} and θ_{2j} using a 1-2 rotation sequence. The orientation of the towed body is defined by using Euler angles, Ψ, Θ, and Φ, in a standard 3-2-1 rotation sequence, as shown in Fig. 2.

The controls assumed for the purposes of this paper are canards for pitch and yaw control (deflections δ_e and δ_r) and ailerons on two wings for roll control (deflection δ_a).

Dynamics

Equations of motion for the system of interest may be derived using several different methods such as direct application of Newton's laws of motion and Lagrange's methods. All of these methods are, of course, based on Newton's laws of motion, but different methods often produce equations of differing algebraic complexity.

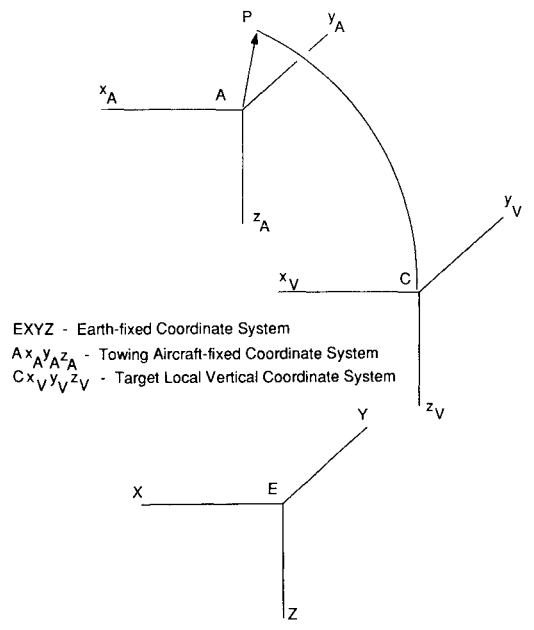

Fig. 1 Coordinate systems: *EXYZ*, Earth-fixed; $Ax_Ay_Az_A$, towing aircraft-fixed; $Cx_Vy_Vz_V$, vehicle-carried local vertical.

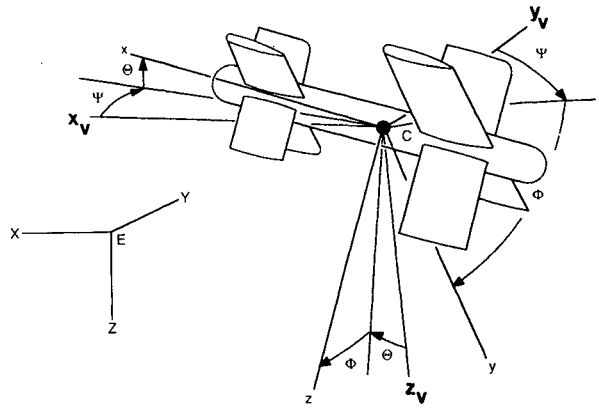

Fig. 2 Towed vehicle orientation.

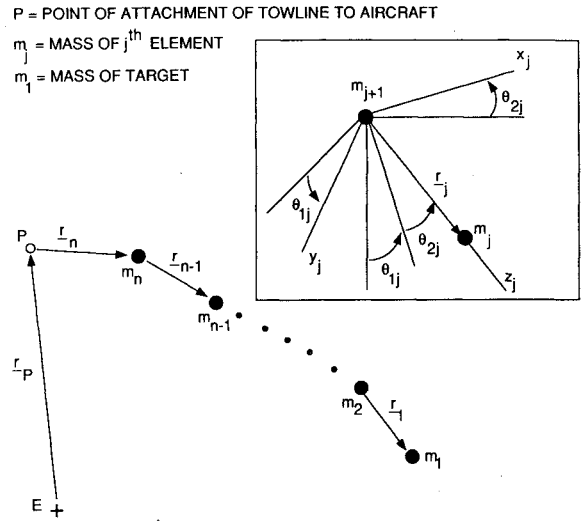

Fig. 3 Lumped-mass cable model; *P*, point of attachment of towline to aircraft; m_j, mass of *j*th element; m_1, mass of target.

In our work on this problem we have actually used two approaches, both based on the direct application of Newton's laws of motion. The differences in the two approaches were in the choice of variables and the method of eliminating constraint forces. Since the cable is assumed inextensible, the constraints of constant length segments must be enforced and the tensions in segments are the constraint forces. To eliminate these forces, we first used cross products of the $\boldsymbol{r}_j$ with equations containing $\boldsymbol{T}_j$, which is colinear with $\boldsymbol{r}_j$. This process led to relatively complicated rigid-body-type equations containing moments of inertia of portions of the system of bodies. A simulation program based on these equations was developed and exercised, and ran very slowly.

To obtain equations that required fewer computations to evaluate derivatives, we selected the following variables:

$$\boldsymbol{v}_j = \boldsymbol{\omega}_j \boldsymbol{x} \boldsymbol{r}_j, \qquad j = 1,2,\ldots,n-1 \tag{1}$$

which are the velocities of the m_j with respect to the m_{j+1}, and $\boldsymbol{v}_n$, the velocity of m_n with respect to *P*. The first $n-1$ of these velocities may be expressed as in Eqs. (1) because the segments between the masses are straight and inextensible. During deployment or retrieval, $\dot{\boldsymbol{r}}_n = \dot{r}_n \hat{\boldsymbol{e}}_{3n}$, and at other times $\dot{r}_n = 0$. For any of the $\boldsymbol{v}_j$, we may write the acceleration of m_j with respect to m_{j+1} (or *P*) as

$$\dot{\boldsymbol{v}}_j = \mathring{\boldsymbol{v}}_j + \boldsymbol{\omega}_j \times \boldsymbol{v}_j \tag{2}$$

where

$$\mathring{\boldsymbol{v}}_j = \dot{u}_{1j}\hat{\boldsymbol{e}}_{1j} + \dot{u}_{2j}\hat{\boldsymbol{e}}_{2j} + \dot{u}_{3j}\hat{\boldsymbol{e}}_{3j}$$

Except for $j=n$, $u_{3j}=0$. The components u_{ij} are suitable variables, and from them we can obtain kinematic equations for the θ_{ij}, $i=1,2$; $j=1,2,\ldots,n$, in the following forms:

$$\dot{\theta}_{1j} = -(u_{2j}/r_j)/\cos\theta_{2j} \tag{3a}$$

and

$$\dot{\theta}_{2j} = (u_{1j}/r_j), \qquad j = 1,2,3,\ldots,n \tag{3b}$$

If we put $\boldsymbol{a}_j = \boldsymbol{a}_P + \Sigma_{k=j}^{n}\dot{\boldsymbol{v}}_k$, where $\boldsymbol{a}_P$ is the acceleration of point P, use $\boldsymbol{A}_j$, $j \geq 1$, to denote the aerodynamic force attributed to the jth segment and acting on m_j, $\boldsymbol{A}_1$ to denote the aerodynamic force on the towed vehicle, and $\boldsymbol{T}_j$ to denote the tension in the jth segment, then the equations for translational motion are

$$\begin{aligned} m_n\boldsymbol{a}_n &= \boldsymbol{T}_n - \boldsymbol{T}_{n-1} + \boldsymbol{A}_n + m_n\boldsymbol{g} \\ m_{n-1}\boldsymbol{a}_{n-1} &= \boldsymbol{T}_{n-1} - \boldsymbol{T}_{n-2} + \boldsymbol{A}_{n-1} + m_{n-1}\boldsymbol{g} \\ &\vdots \\ m_1\boldsymbol{a}_1 &= \boldsymbol{T}_1 + \boldsymbol{A}_1 + m_1\boldsymbol{g} \end{aligned} \tag{4}$$

By adding appropriately selected equations from Eqs. (4), we obtain the following equations, each of which contain only one tension vector:

$$\begin{aligned} m_1\boldsymbol{a}_1 &= \boldsymbol{A}_1 + m_1\boldsymbol{g} + \boldsymbol{T}_1 \\ m_1\boldsymbol{a}_1 + m_2\boldsymbol{a}_2 &= \boldsymbol{A}_1 + \boldsymbol{A}_2 + (m_1+m_2)\boldsymbol{g} + \boldsymbol{T}_2 \\ &\vdots \\ m_1\boldsymbol{a}_1 + \cdots + m_{n-1}\boldsymbol{a}_{n-1} + m_n\boldsymbol{a}_n &= \boldsymbol{A}_1 + \boldsymbol{A}_2 + \cdots + \boldsymbol{A}_n \\ &\quad + (m_1+m_2+\cdots+m_n)\boldsymbol{g} + \boldsymbol{T}_n \end{aligned} \tag{5}$$

Since $\dot{\boldsymbol{v}}_j = \mathring{\boldsymbol{v}}_j + \boldsymbol{\omega}_j \times \boldsymbol{v}_j$, Eqs. (5) provide $3n$ equations for the $2(n+1)+3$ components of the $\boldsymbol{v}_j$, $j=1,2,\ldots,n$. To extract the components, we may take dot products of the equations with appropriate unit vectors.[14] For example, we can multiply the first equation of Eqs. (5) by $\hat{\boldsymbol{e}}_{11}$ and $\hat{\boldsymbol{e}}_{21}$ to obtain equations for u_{11} and u_{21}, respectively. The scalar equations can then be put into the matrix form,

$$\underline{\underline{M}}\dot{\boldsymbol{u}} = \boldsymbol{F} \tag{6}$$

The dot products can be conveniently computed by using direction cosine matrices $\underline{\underline{C}}_j$, which are functions of θ_{1j} and θ_{2j}. For example, $\hat{\boldsymbol{e}}_{ik}\cdot\hat{\boldsymbol{e}}_{j\ell}$ is the element of $\underline{\underline{C}}_k^T\underline{\underline{C}}_\ell$ in the ith row and jth column.

In addition to Eqs. (3) and (6), we need equations that govern the rotational motion of the towed vehicle. Since the tow point on the vehicle for the model discussed here is the vehicle's center of mass, the cable exerts no moment on the vehicle. Thus, the rotational motion equations are simply

$$\underline{\underline{I}}\dot{\boldsymbol{\Omega}} = -\tilde{\boldsymbol{\Omega}}\underline{\underline{I}}\boldsymbol{\Omega} + \boldsymbol{M}_A \tag{7}$$

where $\underline{\underline{I}}$ is the centroidal inertia matrix of the vehicle, $\boldsymbol{\Omega}=(p\ q\ r)^T$ is a matrix of angular velocity components (vehicle-fixed),

$$\tilde{\boldsymbol{\Omega}} = \begin{bmatrix} 0 & -r & q \\ r & 0 & -p \\ -q & p & 0 \end{bmatrix} \tag{8}$$

and $\boldsymbol{M}_A$ is the aerodynamic moment, which we write as $\boldsymbol{M}_A=(L\ M\ N)^T$.

To complete our equations we need the usual[16] kinematic equations for the Euler angles Ψ, Θ, and Φ:

$$\begin{bmatrix} \dot{\Phi} \\ \dot{\Theta} \\ \dot{\Psi} \end{bmatrix} = \begin{bmatrix} 1 & \tan\Theta s\Phi & \tan\Theta c\Phi \\ 0 & c\Phi & -s\Phi \\ 0 & s\Phi/c\Theta & c\Phi/c\Theta \end{bmatrix} \begin{bmatrix} p \\ q \\ r \end{bmatrix} \tag{9}$$

Aerodynamics

Two aerodynamic models for the tow system are needed. The cable aerodynamics will be considered first, followed by a discussion of the towed vehicle aerodynamic model.

For the jth cable segment, the aerodynamic force is modeled by[17]

$$\boldsymbol{A}_j = \left[\tfrac{1}{2}\rho d_{c_j} v_{c_j} C_c \boldsymbol{v}_{c_j} - \tfrac{1}{2}\rho d_{c_j} v_{t_j}^2 \pi C_f \hat{\boldsymbol{t}}_j\right] r_j \tag{10}$$

where ρ is the atmospheric density, d_{c_j} is the diameter of the cable segment, v_{c_j} is the magnitude of the crossflow velocity $\boldsymbol{v}_{c_j}$, C_c is the crossflow drag coefficient, v_{t_j} is the magnitude of the tangential velocity $\boldsymbol{v}_{t_j}$, C_f is the skin-friction coefficient, $\hat{\boldsymbol{t}}_j = \boldsymbol{T}_j/T_j = \hat{\boldsymbol{e}}_{3j}$, and r_j is the length of the segment. The coefficients C_c and C_f are, in general, functions of the local Mach number. The crossflow velocity is found from $\boldsymbol{v}_{c_j} = \boldsymbol{v}_{RW_j} - (\boldsymbol{v}_{RW_j}\cdot\hat{\boldsymbol{e}}_{3j})\hat{\boldsymbol{e}}_{3j}$, where $\boldsymbol{v}_{RW_j} = \boldsymbol{v}_P + \Sigma_{k=j}^{n}\boldsymbol{v}_k$. The aerodynamic force on the towed vehicle is assumed to be of the standard form, $\boldsymbol{A}_1 = X\hat{\boldsymbol{i}} + Y\hat{\boldsymbol{j}} + Z\hat{\boldsymbol{k}}$. The components X, Y, and Z can be expressed in terms of the coefficients C_x, C_y, and C_z, respectively. These may, in turn, be expressed in terms of standard stability derivatives, the vehicle angle of attack α, and the sideslip angle β.

We assume that the position velocity and acceleration of the point P are known. Thus, to define the location of the towed vehicle's center of mass, we may use

$$\boldsymbol{r}_c = \boldsymbol{r}_p + \sum_{j=1}^{n}\underline{\underline{C}}_j(0\ 0\ r_j)^T \tag{11}$$

In the simulation the equilibrium states corresponding to a particular towing speed are calculated from the equations $\boldsymbol{F}_e = \boldsymbol{0}$ and $\boldsymbol{M}_{A_e} = \boldsymbol{0}$. When the flowfield in which the towed vehicle is submerged can be considered uniform, then for given equilibrium angles of attack (α_e) and sideslip (β_e) of the vehicle, control deflections for trim can be found from the moment equation $\boldsymbol{M}_A = \boldsymbol{0}$. The force $\boldsymbol{A}_1$ may be computed, followed by $\boldsymbol{T}_{1_e}$ and the angles θ_{11_e} and θ_{21_e}. Then $\boldsymbol{A}_{2_e}$, $\boldsymbol{T}_{2_e}$, etc., on up the cable to point P can be determined. When the flowfield is nonuniform but steady, an iterative procedure may be employed to find equilibrium solutions.[14]

III. Control System

For the purpose of this paper the control system was synthesized using a linear short-period dynamic model of the unconstrained (no cable) vehicle. The control system was tested in the nonlinear simulation to verify its proper operation. The system is similar to the system used in the vehicle described in Ref. 14.

The objectives established for the autopilot of the towed vehicle were to achieve good stability characteristics at the trim in the presence of external disturbances and to allow for good maneuverability in changing trim conditions. The autopilot consists of three components: 1) an inner SCAS, 2) a maneuver autopilot (MA) to control the process of moving the vehicle from one trim condition to a new one, and 3) a stationkeeping autopilot (SKA). In this section the characteristics of the three autopilot components are described, and design parameters are given for a typical flight condition.

Stability and Control Augmentation System

The SCAS is the inner loop of the autopilot and must provide adequate stability and quickness characteristics and be

insensitive to sensor/actuator errors and uncertainties in aerodynamic parameters.

The SCAS structure is traditional; the design was performed using classical control techniques and linear analysis. Although the motion of the towed vehicle is affected by the motion of the parent aircraft, as stated earlier, for the purpose of synthesizing the SCAS, we assumed that the vehicle was free and used standard linearized dynamics, including the three rotations (roll, pitch, and yaw) and vertical and lateral translations. Geometric, mass, and aerodynamic data for the hypothetical vehicle used in the synthesis process are given in Table 1 for a reference speed of 100 m/s and sea-level conditions.

The SCAS consists of three subsystems, one for each axis (x = roll, y = pitch, z = yaw). The controllers in pitch and yaw are similar in structure, the only difference being a sign change due to the standard convention used in defining sideslip and angle of attack.

Roll SCAS

The main requirement of this subsystem is to provide roll stabilization in the presence of external disturbances and sensor/actuator errors. A secondary objective is to achieve good command following if a particular roll angle is desired (especially during deployment and retrieval if a nonzero roll angle is necessary for saddle locking).

A block diagram of the roll autopilot is shown in Fig. 4. The vehicle dynamics are given by the traditional first-order roll approximation

$$\phi(s) = G_\phi \delta_A + \frac{G_\phi}{a} D \tag{12}$$

where

$$G_\phi = a/[s(s+b)] \tag{13}$$

$$a = 498.42, \qquad b = 5.35$$

Table 1 Vehicle characteristic parameters

Parameter	Value	Parameter	Value
Mass m	30.91 kg	C_{L_α}	51.57
Length ℓ	1.76 m	C_{m_α}	−70.69
Ref. area S	0.0324 m^2	C_{m_q}	−1173.87
Ref. length $\bar{c}$	0.203 m	$C_{L_{\delta_E}}$	5.66
x_{cg}	0.889 m	$C_{m_{\delta_E}}$	37.48
I_x	1.2558 kg-m^2	C_{ℓ_p}	−160.61
$I_y = I_z$	10.563 kg-m^2	$C_{\ell_{\delta_A}}$	15.2
Ref. speed v_0	100 m/s	ρ	Sea level

Table 2 Roll controller data

Parameter	Value	Parameter	Value
K'_{ACT}	$3K_{ACT}$	$1/T_c$	0.6
K'_{VG}	$10K_{VG}$	$1/\alpha T_c$	0.1
K_{c2}	$1/K'_{VG}$	$1/T_b$	5.35
Gain margin	17 dB	$1/\beta T$	100
Phase margin	70 deg		

Table 3 Pitch controller data

Parameter	Value
K_1	3.5
K_2 ($=1/K_1$)	0.2857
K_3	35
K_z	−0.1
GM, PM, inner loop	≈15 dB, 110 deg
GM, PM, outer loop	≈25 dB, 60 deg

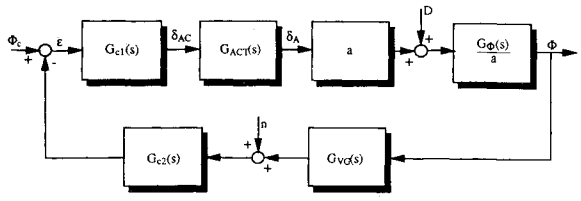

Fig. 4 Roll autopilot block diagram.

and where D is the maximum expected external torque, assumed to be a constant equal to the steady-state rolling moment generated by the maximum aileron deflection. In the present analysis $D = 27.3$ N-m. In Fig. 4, Φ_c is the roll angle command (usually equal to 0 deg), and n is the sensor offset. The sensor is a vertical gyro modeled by a gain $G_{VG}(s) = K_{VG}$ and has a maximum offset, $n = 1$ deg.

We model the actuator, a dc motor, as a linear second-order system with bandwidth $\omega_{ACT} = 10$ Hz and with an error ϵ proportional to the input signal δ_{AC}. The actuator output δ_A is therefore determined by

$$\delta_A = G_{ACT}(s)\delta_{AC} = \left(\frac{K_{ACT}\omega_{ACT}^2}{s^2 + 2\zeta\omega_{ACT}s + \omega_{ACT}^2} + \epsilon\right)\delta_{AC} \tag{14}$$

The actuator gain K_{ACT} has a nominal scale factor value of 2 deg/V. Both actuator and vertical gyro gains can be adjusted for good steady-state performance.

The control system consists of a lag-lead compensator in the forward path, $G_{c1}(s)$, a feedback gain, K_{c2}, and adjusted actuator and gyro gains, K'_{ACT}, K'_{VG}. The lag-lead compensator has the standard structure

$$G_{c1}(s) = \frac{(T_c s + 1)(T_b s + 1)}{(\alpha T_c s + 1)(\beta T_b s + 1)}, \qquad \alpha > 1, \qquad \beta < 1 \tag{15}$$

The lag component is designed to provide a sufficiently high loop gain at low frequency and a good gain margin. The lead component is designed to allow sufficient damping and canceling of the roll mode and additional rolloff at high frequency.

The various gains, K'_{ACT}, K'_{VG}, and K_{c2}, are computed to yield good steady-state response characteristics. In particular, K'_{ACT} is based on the response to the external disturbance D; i.e.,

$$\phi^{ss} = \frac{1}{K'_{ACT}K_{c2}K'_{VG}} D$$

where K_{c2} is equal to $1/(K'_{VG})$ in order to provide zero steady-state error to bank angle command, as shown by the following:

$$\phi^{ss} = \frac{1}{K_{c2}K'_{VG}} \phi_c \tag{16}$$

Finally, the gyro gain is adjusted to minimize the response to its own offset:

$$\phi^{ss} = -\frac{1}{K'_{VG}} n \tag{17}$$

Table 2 gives the numerical values of the controller parameters. The open-loop frequency response exhibits a gain margin of ~17 dB and a phase margin of ~70 deg.

Figure 5 shows the roll-angle time histories in response to an external disturbance and a roll-angle command and sensor offset. As can be seen, satisfactory results are obtained. The control activity in terms of aileron deflection rate, although not shown, is well within the operational limits of conventional actuators.

Pitch SCAS

The pitch channel of the SCAS must provide satisfactory acceleration following with good transient characteristics and stability margins. The pitch SCAS uses a rate gyro and accelerometer combination to generate elevator deflection commands. The inner loop consists of a pseudo-attitude feedback with forward integration to improve the short-period dynamics and to provide zero steady-state error. The center loop consists of integral feedback of acceleration error for good command following. The block diagram of the control system is shown in Fig. 6.

The vehicle transfer functions may be found using the data given in Table 1. Explicitly, we have

$$G_q(s) = \frac{q}{\delta_e} = \frac{146.12(s+4.08)}{s^2+8.03s+291.29} \tag{18a}$$

and

$$G_\alpha(s) = \frac{\alpha}{\delta_e} = \frac{-0.371(s-388.96)}{s^2+8.03s+291.29} \tag{18b}$$

The system is lightly damped ($\zeta = 0.235$) and has a natural frequency of 17.07 rad/s.

A pure gain [i.e., $G_{RG}(s) = K_{RG}$] is used to model the rate gyro. The accelerometer is modeled as a first-order system with a break frequency of ~ 30 Hz, so that

$$G_{ACC} = K_{ACC}\frac{188.4}{s+188.4} \tag{19}$$

Nominally, $K_{RG} = 1$ V/deg and $K_{ACC} = 1/9.8$ (V-s^2)/m.

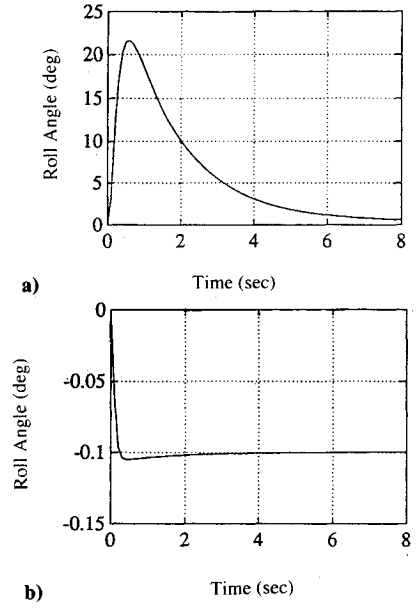

Fig. 5 Rolls response to a) 1-N-m external disturbance; b) 1-deg sensor offset.

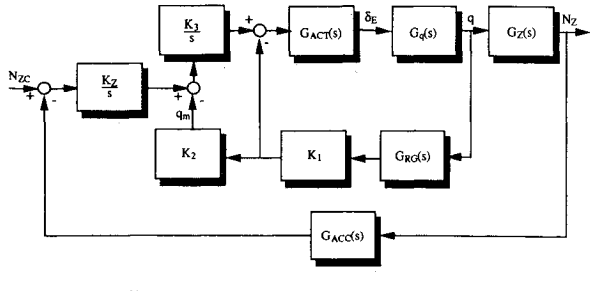

Fig. 6 Pitch autopilot block diagram.

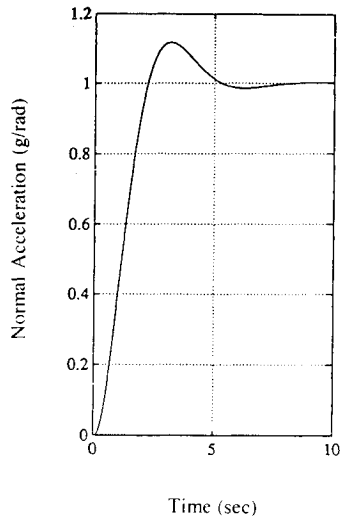

Fig. 7 Normal (z-axis) acceleration response to step command.

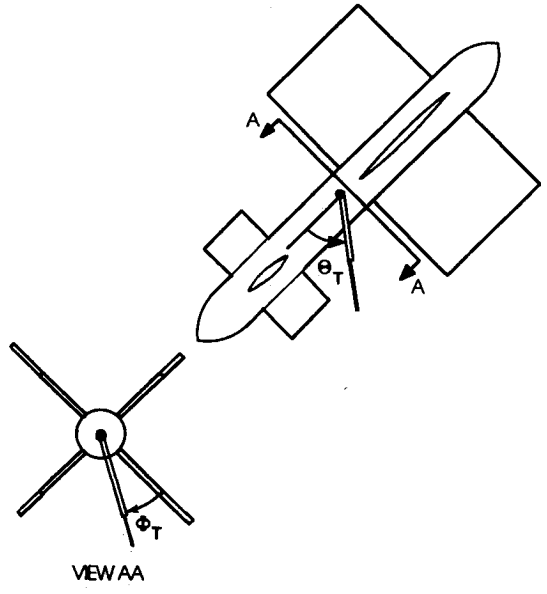

Fig. 8 Cable attachment geometry.

Controller parameters and results for the inner- and outer-loop frequency responses are given in Table 3. The frequency responses indicate good stability margins.

The normal acceleration response to step input command is shown in Fig. 7. This, and the corresponding time histories for pitch rate, yaw rate, etc., are considered satisfactory, since no requirements were set on the time constant and the bandwidth of the system.

The yaw SCAS is similar to the pitch SCAS. The yaw rate r replaces pitch rate q, and $-\beta$ replaces the angle of attack α. The controller gains are the same as those given in Table 3, except that $K_y = 0.1$ is used in the lateral acceleration loop instead of $K_z = -0.1$.

Maneuvering and Stationkeeping

The MA is used to move the towed vehicle from one trim condition to another using a priori estimates of the steady-state control deflections required to achieve a particular trim point. We can write the total control surface deflection (either elevator or rudder) as

$$\delta_c = \delta_{c_1} + \delta_{c_2} \tag{20}$$

where δ_{c_1} is the component due to the SCAS, and δ_{c_2} is the component due to either MA or SKA. Tables of values for δ_{c_2}

are assumed to be available for a given towed vehicle for the particular flight speeds, tow system geometries, and tow aircraft vortex fields of interest.

Once the MA has brought the vehicle near the new trim position, the SKA maintains it near that position by using a priori estimates of the tow cable angle Φ_T, measured at the vehicle, and the two cable tension T, measured at the towing aircraft. The latter measurement is used to provide indirect feedback of the angle Θ_T, as shown in Fig. 8.

The maneuver and stationkeeping algorithms accept current time t, initial and final trim conditions (subscripts 1 and 2), maneuver time t_M; delay time t_o, and tow cable angle and tension gains K_{Φ_T} and K_T as inputs.

The input for a typical maneuver is a smooth deflection command:

$$\delta_{c_2} = \tfrac{1}{2}(\delta_2 - \delta_1)\left\{1 - \cos\left[\pi(t - t_1)/t_M\right]\right\} + \delta_1 \qquad (21)$$

Since the MA is basically open loop and time histories of q, r, N_z, and N_y are not known beforehand, during the maneuver, the SCAS must not respond to long-term changes of the aforementioned variables. Washout circuits were added to the basic autopilot for this purpose. As the maneuver is finished, the gains and/or sensed errors are phased in as the maneuver-related transients in angular rates and accelerations subside.

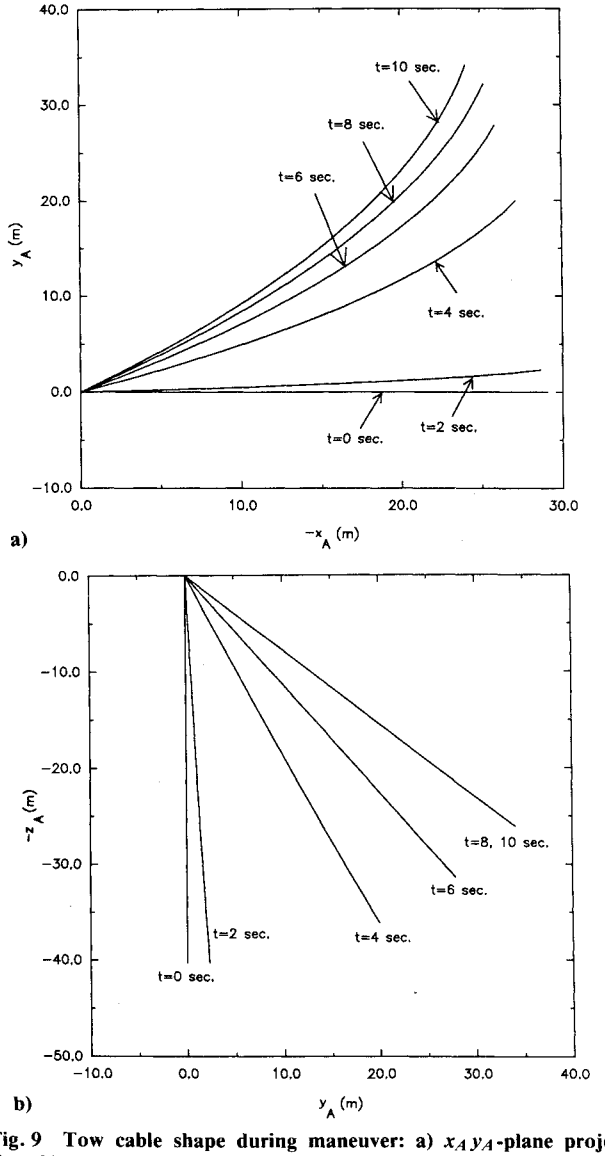

Fig. 9 Tow cable shape during maneuver: a) $x_A y_A$-plane projection; b) $y_A z_A$-plane projection.

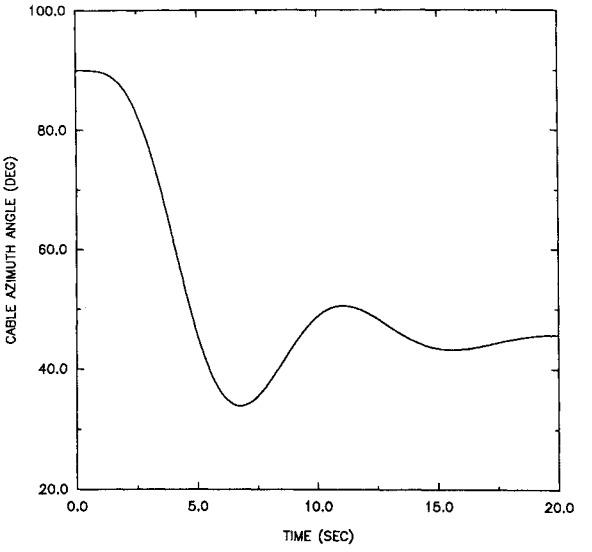

Fig. 10 Tow cable angle Φ_T during maneuver.

IV. Simulation and Results

Simulation Overview

A digital computer program was written (primarily by the third author) to solve the nonlinear system equations and implement the controllers and guidance algorithms. Note that the terms "cable" and "towline" are used synonymously. Either linear or nonlinear aerodynamic models can be used. Two integration routines, a standard fourth-order Runge-Kutta (RK4) and an Euler, are included. The latter routine is used in simulating a digital autopilot, if used. The simulation capabilities include:

1) Options for computing
   a) Steady-state cable configurations and target trim states in
      Uniform flowfield
      Nonuniform flowfield
   b) Dynamic behavior of deployed cable target system, including
      Response to perturbations
      Response to control inputs
      Controlled maneuvers of target
      Maneuvers of tug aircraft
   c) Dynamic behavior of cable/target system during deployment and retrieval of target
2) Stability augmentation can be investigated
3) Guidance (maneuver) laws can be tested

Results

Space limitations preclude the reproduction of results that illustrate all of the simulation's capabilties; thus, we have chosen two cases that illustrate some of what can be simulated. The pitch and yaw controllers described in Sec. III were used to obtain the results for controlled motion given here. The roll autopilot channel used did not include the compensator; i.e., we took $G_{c_1}(s) = 1$. The aerodynamic (linear model) and physical data used are those for the vehicle given in Sec. III and those for the cable, which are listed as follows:

1) Cable diameter d_c, 0.0239 ft
2) Weight per unit length σ, 0.04 lb/ft
3) Crossflow drag coefficient

$$C_c = 1.17 + M_n/40 - M_n^2/4 + 5M_n^3/8$$

4) Skin-friction drag coefficient

$$\pi C_f = \begin{cases} 0.038 - 0.0425 M_p, & M_p < 0.4 \\ 0.013 + 0.0395\ (M_p - 0.85)^2, & M_p \geq 0.4 \end{cases}$$

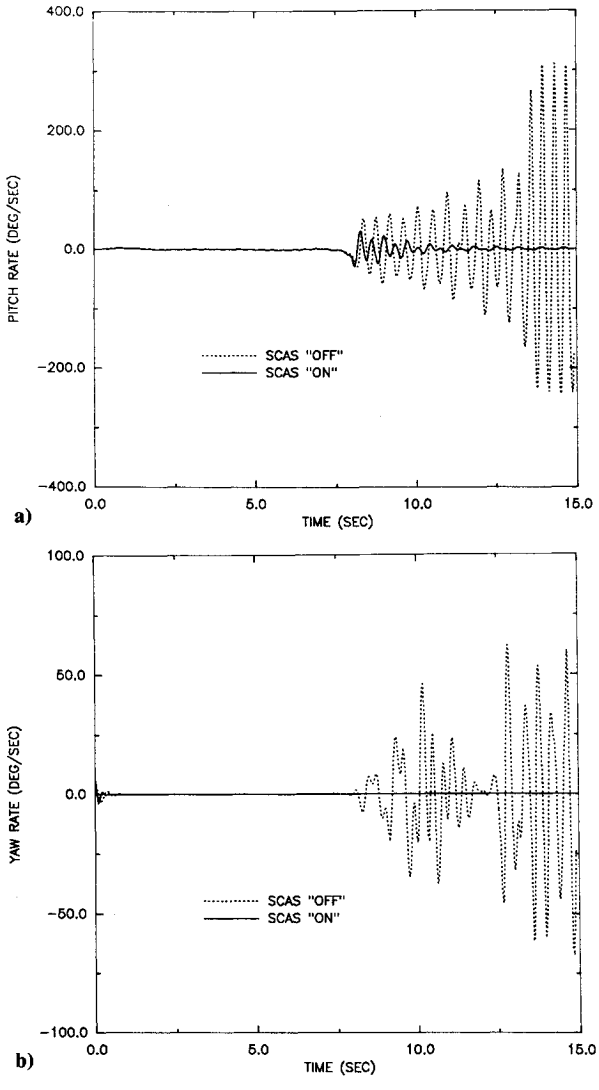

Fig. 11 Towed vehicle angular rates during retrieval: a) pitch rate; b) yaw rate.

5) M_n, Mach number normal to the cable segment; M_p, Mach number parallel to the cable segment.

Case 1: Maneuver out of the Vertical Plane

Case 1 illustrates the capability of the simulation and the control and guidance algorithms to handle a lateral maneuver of the vehicle from a point to the rear and beneath the tow point P to a position 45 deg clockwise from that point as viewed from behind the towing aircraft. Figures 9a and 9b show the projections of the cable onto the $x_P y_P$ and $y_P z_P$ planes during the 4-s maneuver, a 2-s settling period, and a 4-s stationkeeping time. The cable azimuth angle Φ_T time history is shown in Fig. 10. The desired final value of 45 deg was reached to within ± 5 deg in ~ 12 s.

Case 2: Retrieval

Whereas the first case indicates the well-behaved motion of the towed vehicle, this retrieval case shows that uncontrolled motion of the vehicle may not be sufficiently stable when the retrieval is stopped at a length of 0.6 m. Just before retrieval began, the motion of the vehicle was slightly perturbed by putting in a 0.1-rad/s yaw rate. Retrieval from 50 m to 0.6 m took 8 s. The retrieval rate was of the following form:

$$\dot{r}_n = \begin{cases} (\dot{r}_{\max}/2.)\left[1-\cos(\pi t/t_1)\right], & 0 \le t \le t_1 \\ \dot{r}_{\max}, & t_1 < t < t_2 \\ (\dot{r}_{\max}/2)\left[1-\cos\pi(t-t_2+t_1)/t_1\right], & t_2 \le t \end{cases}$$

where $\dot{r}_{\max} = 24.05$ m/s, $t_1 = 2$ s, and $t_2 = 7$ s. The simulation continued for 7 s after the retrieval rate became 0. Figures 11a and 11b show the time histories of vehicle pitch rate and yaw rate, respectively, for SCAS off and SCAS on conditions. Note that, with the SCAS off, the pitch rate amplitude of the towed vehicle continuously increased after retrieval was stopped at $t = 8$ s. A small pitch rate disturbance occurred at $t = 7$ s when the retrieval rate started to decrease. The yaw rate amplitude exhibits a beat-type behavior. With the SCAS on, the motion of the vehicle in pitch and yaw is stable in an asymptotic sense. The cable configurations at various times are shown in Fig. 12. At the end of retrieval the vehicle swings back and forth somewhat. However, in an actual application the vehicle would probably be captured in a cradling mechanism.

V. Comparison with Experimental Results

To compare theoretical and experimental results as an additional check on the validity of our model, the third author developed a version of the simulation that models the vehicle with the tow cable connected at an arbitrary position rather than at its center of mass. We used this more general simulation to produce results for comparison with particular experimental and theoretical lateral stability boundaries given in Ref. 8. For this work we used $n = 5$. The wind speed was

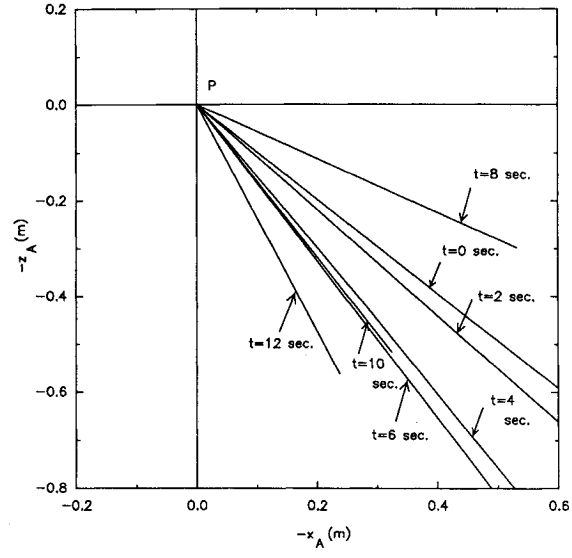

Fig. 12 Tow cable shape during retrieval: $x_A z_A$ projection.

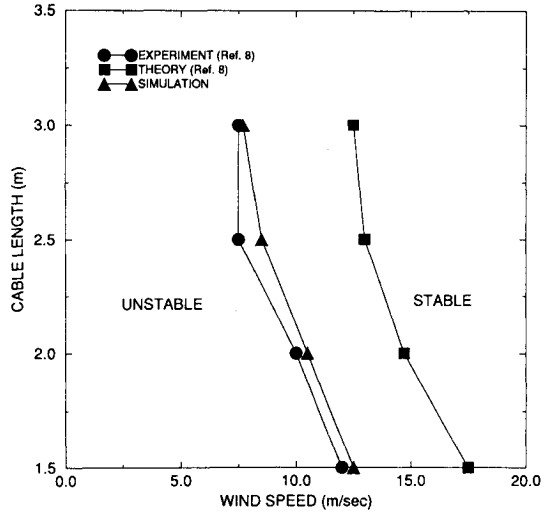

Fig. 13 Lateral motion stability boundaries for a small tethered wind-tunnel model.

varied for a given cable length until a sustained, constant-amplitude, lateral oscillation was achieved using the simulation. Pairs of values of speed and cable length at which such oscillations occur were used to define a stability boundary. Figure 13 shows three types of results, the experimental and theoretical results of Ref. 8 and our theoretical results. We note that in this case the present simulation predicts the experimentally determined stability boundary much more accurately than the linear theory of Ref. 8.

VI. Conclusions

The problems of modeling the dynamics of a towed flight vehicle system and of designing a system for automatically controlling the vehicle's motion have been addressed. A multibody model of the cable and towed vehicle has been developed that includes provisions for arbitrary towing aircraft motion and deployment, retrieval, maneuvering, and stationkeeping of the towed vehicle. Classical control theory has been applied to design a stability and control augmentation system. A maneuver (guidance) autopilot and a stationkeeping autopilot based on system geometry have also been developed. A digital simulation program that incorporates all of the models has been written and used to simulate the motion of a typical maneuvering target. Sample results from the simulation have been presented. These results include a comparison of a lateral stability boundary obtained by using the simulation with one determined experimentally. Very good agreement was achieved. The simulation has been used in the successful development of a maneuverable tow target.

Acknowledgments

We gratefully acknowledge financial support for this work by Hayes Targets and beneficial technical discussions with Hugh B. Feagle and Denton Marlow.

References

[1]Glauert, H., "The Stability of a Body Towed by a Light Wire," Aeronautical Research Commitee (Great Britain) Repts. and Memo No. 1312, Feb. 1930.

[2]Phillips, W. H., "Stability of a Body Stabilized by Fins and Suspended from an Airplane," NACA ARR L4D18, 1944.

[3]Phillips, W. H., "Theoretical Analysis of Oscillations of a Towed Cable," NACA TN 1796, 1949.

[4]Genin, J., and Cannon, T. C., "Equilibrium Configurations and Tensions of a Flexible Cable in a Uniform Flow Field," *Journal of Aircraft,* Vol. 4, No. 3, 1967, pp. 200–202.

[5]Norman, R. I., Morrow, V. E., Hamer, W. S., and St. John, D. L., "The Maneuvering Tow System," Hayes International Corporation, Hayes Engineering Rept. 1500, Birmingham, AL, 1968.

[6]Huffman, R. R., and Genin, J., "The Dynamical Behavior of a Flexible Cable in a Uniform Flow Field," *Aeronautical Quarterly,* May 1971, pp. 183–195.

[7]Huang, S. L., "Mathematical Models for a Long Cable Towed by Orbiting Aircraft," Naval Air Development Center, Rept. NADC-AM-6849, Johnsville, Warminster, PA, June 1969.

[8]DeLaurier, J. D., "A First Order Theory for Predicting the Stability of Cable Towed and Tethered Bodies Where the Cable has a General Curvature and Tension Variation," von Kármán Institute for Fluid Dynamics, TN 68, Rhode-Saint-Genese, Belgium, Dec. 1970.

[9]Cannon, T. C., and Genin, J., "Towed Vehicle System in a Coordinated Turn," *AIAA Journal,* Vol. 10, No. 3, 1972, pp. 252–257.

[10]James, S. P., and Krausman, J. A., "Nonlinear Dynamic Simulation of a Tethered Aerostate," *Journal of Aircraft,* Vol. 17, No. 8, 1982, pp. 679–686.

[11]Misra, A. K., and Modi, V. J., "Deployment and Retrieval of Shuttle Supported Tethered Satellites," *Journal of Guidance, Control, and Dynamics,* Vol. 5, No. 3, 1982, pp. 278–285.

[12]Kane, T. R., and Levinson, D. A., "Deployment of a Cable-Supported Payload from an Orbiting Spacecraft," *Journal of Spacecraft and Rockets,* Vol. 14, No. 7, 1977, pp. 438–444.

[13]Kirschner, L. R., "The Skyhook Program: A Software Package for a Tethered Satellite System, Including Electrodynamic Interactions," Smithsonian Institution, Astrophysical Observatory, Contract NAS8-33691, Cambridge, MA, May 1980.

[14]Cochran, J. E., Jr., Innocenti, M., No, T. S., and Thukral, A., "Six Degree-of-Freedom Simulation and Performance Analysis for the TRX-12 Tow Target, Final Report, Vol. II, Simulation," Hayes Targets, Contract 927047-A, Leeds, AL, March 22, 1990.

[15]"Hayes Officials Study New Uses for Software-Maneuverable Tow Targets," *Aviation Week & Space Technology,* June 24, 1991, p. 42.

[16]Etkin, B., *Dynamics of Flight—Stability and Control,* 2nd ed., Wiley, New York, 1982, Chaps. 4 and 5, p. 10.

[17]Burkhalter, J. E., Dasher, T. E., and Wilder, G. O., "Six Degree-of-Freedom Simulation and Performance Analysis for the TRX-12 Tow Target, Final Report, Vol. I, Aerodynamics," Hayes Targets, Contract 927047-B, Leeds, AL, Sept. 30, 1989.